Astron. Astrophys. 346, 936–946 (1999)

ASTRONOMY AND ASTROPHYSICS

Distribution of gas, dust and the λ6613 Å DIB carrier in the Perseus OB2 association⋆

P. Sonnentrucker[1,2], **B.H. Foing**[2,3], **M. Breitfellner**[4], **and P. Ehrenfreund**[5]

[1] Observatoire de Strasbourg, 11 rue de l'Université, F-67000 Strasbourg, France
[2] Solar System Division, ESA Space Science Department, ESTEC/SO, PB 299, 2200 AG Noordwijk, The Netherlands
[3] Institut d'Astrophysique Spatiale, CNRS, Bat 121, Campus d'Orsay, F-91405 Orsay, France
[4] ISO Data Center, Astrophysics Division, Space Science Department of ESA, Villafranca, P.O. Box 50727, E-28080 Madrid, Spain
[5] Leiden Observatory, P.O. Box 9513, 2300 RA Leiden, The Netherlands

Received 16 December 1998 / Accepted 12 March 1999

Abstract. We present a study of the spatial distribution of the λ6613 Å DIB carrier in the Perseus OB2 association based on high resolution observations toward lines of sight representing different interstellar environments. We determined that in the studied region, the λ6613 Å DIB carrier is concentrated in two distinct clouds with velocities of 1.4 ($\pm$ 0.4) and 12.0 ($\pm$ 0.9) km s^{-1}. We compared the λ6613 Å DIB carrier's velocity with the Na I velocity distribution derived from our survey measurements, as well as with CO, OH, H I and Ca II measurements from the literature. We conclude that the behaviour of the carrier of the λ6613 Å DIB follows the overall expansion motion of the gas in the association. The DIB velocity is directly linked to that of Ca II and H I. The DIB total column density is proportional to the total column density of Ca II and H I making those atoms good tracers of the λ6613 Å DIB carrier. Those new results support the assumption that the λ6613 Å DIB would arise from a gas phase molecule, possibly single-ionized (Sonnentrucker et al. 1997). We also conclude that the DIB carrier is distributed in shell structures over the whole association. We finally show from the DIB velocity structure that the DIB carrier, gas and dust are well mixed toward the association but that the DIB shells have an angular extent twice larger than that of the dust.

Key words: line: profiles – ISM: clouds – ISM: dust, extinction – ISM: lines and bands – ISM: molecules

1. Introduction

The Diffuse Interstellar Bands (DIBs) are weak absorption features detected in the visible range toward reddened OB stars (Herbig, for a review 1995). Additional searches for DIBs in the UV and NIR were recently performed. At the present time, two diffuse bands were detected in the NIR ($\lambda\lambda$9577 and 9632 Å) showing consistency with laboratory spectra of the fullerene cation, C_{60}^{+} (Foing & Ehrenfreund 1994, 1997). Coincidences of laboratory measurements on PAH cations have been reported by Salama et al. (1996). C-chains are also discussed as possible carriers for some DIBs (Tulej et al. 1998). However, most of the remaining DIBs (currently more than 250, Ó Tuairisg 1998) still arise from unidentified carriers. DIBs were first thought to originate in dust grains due to the correlation of the band's strength with the line-of-sight reddening. Further observations and recent investigations definitely point toward a gas phase molecular origin for several DIBs. Attempts to group DIBs into families were made assuming that similar DIB behaviour traces similar molecular carriers (Krelowski & Walker 1987). Cami et al. (1997) recently showed that the λ6613 Å DIB correlates with a few DIBs, among them are the $\lambda\lambda$5797 and 6379 Å DIBs. Those DIBs seem to have individual but very similar molecular carriers.

Large DIB surveys showed that DIBs are weak in Photon-Dominated Regions (PDRs) and in dense molecular clouds, suggesting that the DIBs strength depends upon the physical and chemical properties of the interstellar clouds (Snow & Cohen 1974, Adamson et al. 1991, Jenniskens et al. 1994, Krelowski et al. 1996). This fact was recently interpreted as a change of the charge state of the DIB carriers in different environments and led Sonnentrucker et al. (1997, 1998) to Ionization Potential (IP) estimations for possible carrier molecules. For the λ6613 Å DIB carrier an IP between 10 and 13 eV was estimated, consistent with a single-ionized PAH or fullerene-type molecule.

High resolution spectroscopy revealed the presence of substructures in a few DIB profiles (Sarre et al. 1995, Ehrenfreund & Foing 1996, Krelowski & Schmidt 1997, Kerr et al. 1996, 1998). The λ6613 Å DIB exhibits a triple peaked profile. Comparison of rotational contour calculations with observed DIB profiles suggests that the λ6613 Å DIB may originate in a large gas phase molecule containing between 12 to 40 C atoms, depending on the model assumed for the potential carrier (PAH, fullerenes, C-chains, C-rings, see Ehrenfreund & Foing 1996).

We performed high resolution observations of the λ6613 Å DIB in 6 well known lines of sight of the Perseus OB2 association, in order to study the DIB spatial distribution. We investigated the possible link of the λ6613 Å DIB with the distribution

Send offprint requests to: P. Sonnentrucker

⋆ Based on observations with OHP 1.52m Telescope and Aurélie spectrograph.

of atoms and molecules which trace the gas and the dust as well as the physical conditions reigning in those interstellar regions.

The sections are organized as follows: Sect. (2) describes the data acquisition, reduction and fitting procedures used for this work, Sect. (3) discusses the conclusions drawn about the distribution of the λ6613 Å DIB and the implications on the nature of that particular DIB carrier.

2. Data reduction

2.1. Observations

Observations were performed in November 1996 and December 1997. We used the high resolution facilities offered by the 1.52m Coudé telescope and the Aurélie Spectrograph, installed at the 'Observatoire de Haute-Provence' (OHP), France. We reached a resolving power of R=110 000, using the 'Echelle' grating together with available interference filters. The wavelength ranges were centered at λ_c=3934, 5895 and 6613 Å. Our spectral resolution was 2.8 ($\pm$ 0.3) km s^{-1}. The spectral coverage in each wavelength range was about 27, 38 and 45 Å, respectively, permitting to observe the Na I doublet (λ5890 and λ5895 Å) and the λ3934 Å component of the Ca II doublet. We completed our data sample with literature measurements from previous Ca II and Na I surveys when necessary (see Table 2).

The 6 Perseus targets were observed in sequence with the spectral type standard HD23630 and the telluric standards HD25642 and HD120315 to allow an optimized correction of spectral and/or telluric line contaminations. The 3 other targets were observed in sequence with the standards HD205021 and HD40111.

The study of the λ6613 Å diffuse band requires high S/N ratios to detect any profile variation. We reached S/N ratios up to 450 with exposure times ranging from 25 to 60 min for stars with V magnitudes between 3.8 and 6.6. S/N ratios of 100 and 200 were obtained for the Na I and Ca II lines, respectively, which are sufficient to detect multiple-cloud components. Table 1 summarizes the known parameters concerning the 9 sample targets. For each line of sight we reported, respectively, the: (0) literature references used, (1) star name, (2) reddening, (3) rotational temperature of molecular hydrogen, (4) galactic longitude, (5) galactic latitude, (6) average Hipparcos distance of each target, (7) Hipparcos distance error range, (8) photometric distance (Černis 1993) and (9) spectroscopic distance from Guetter (1977). The 3 last stars of Table 1 were added to the Perseus sample to study the DIB profile variations and attempt to link them to the rotational temperature variations from one line of sight to another. This issue will be discussed in another study.

2.2. Data reduction

We corrected all spectra from bias and flatfield effects. We removed possible stellar and/or telluric contaminations by dividing the spectrum of each program star by the spectrum of its corresponding standard star. Each division was scaled with the appropriate airmass ratio. The Na I and 2 Ca II spectra obtained during our campaigns were also corrected by division using the telluric standard HD120315 (η UMa) to remove line contaminations due to atmospheric water vapor. The data reduction was performed during the observing runs with the help of installed IHAP routines. Those preliminary reductions were checked and refined later. The wavelength calibration was performed using IDL procedures.

We computed the heliocentric velocity corrections for each line of sight with the MIDAS routine "Barycorr". To allow a comparison between the DIB and Na I spatial distributions from our sample with the Ca II, H I, OH and CO literature data from previous surveys, we took the following air rest wavelengths: $\lambda_{\rm DIB}$ = 6613.62 Å (Herbig 1995), $\lambda_{\rm Na\,I}$ = 5895.9242 Å (Welty et al. 1994) and $\lambda_{\rm Ca\,II}$ = 3933.663 Å (Welty et al. 1996). The CO cloud velocity components were taken from Ungerechts & Thaddeus (1987) and Smith et al. (1991), the H I and OH velocities come from Sancisi et al. (1974).

2.3. Fitting procedure

We fitted the data using IDL procedures. The function required by the procedure was set as the sum of a 2 degree polynom and 1 to 4 gaussian functions, depending on the complexity of the profile and the purpose of the fit.

All Full Width at Half Maximum (FWHM) of the DIB lines as well as all "centroid velocity" ($V_{\rm C}$) measurements were derived from *one-gaussian* fits.

The 5 Na I, 2 Ca II and 9 DIB profiles were fitted via *multiple-gaussian* fits to reproduce the cloud velocity structures of the atomic lines as well as the substructures in the DIB profiles. The fitting procedure was performed in two steps for each line of sight.

Each spectrum was fitted a *first time* providing a set of *12 to 15 initial parameters* per spectrum, depending on the shape of the profile. Each spectrum data point s(i) was given a weight $w(i) = 1/d(i)^2$, where $d(i)$ is the residual and $f(i)$ the fit result at data point (i). We set the residuals to a fixed value of 0.003, the convergence tolerance to 10^{-4}. The results of the first fit were then used as new initial parameters to refine the fitting procedure.

A summary of the results can be found in Table 2. $V_{\rm P1}$ to $V_{\rm P3}$ represent the fits of the λ6613 DIB triple-peak substructure. The peaks are reported with increasing velocity. The Na I velocity distribution ($V_{\rm Na\,D1}$) is derived from our measurements, except for HD24398 (Welty et al. 1994). We reported the dominant Na I cloud positions when necessary. Welty et al. (1996) achieved a resolution $\sim$9 times higher than ours (Δv = 0.32 against 2.8 km s^{-1}). To allow comparison between their sample and ours, we calculated the weighted mean of Welty's resolved Ca II components ($V_{\rm Ca\,IIwm}$), each component being weighted by its corresponding column density. The CO velocity distribution is also reported when available (Ungerechts & Thaddeus, 1987 and Smith et al. 1991).

We also calculated the DIB weighted mean velocity ($V_{\rm DIBwm}$), using the 3 substructure velocities, weighting each peak with its corresponding equivalent width. The velocity dis-

Table 1. Line of sight parameters for the program stars. We reported from top to bottom the: literature references (see footnote), star name, reddening ($E_{(B-V)}$), H_2 rotational temperature (T_{01}), star galactic longitude (l°) and galactic latitude (b°), Hipparcos distance (D) and its error range (Err_D), photometric distance D_{ph}, spectroscopic distance D_{sp}.

Ref	HD	24760	22951	23478	24912	23180	24398	218376	2905	41117
1	Name	ϵ Per	40 Per	-	ξ Per	o Per	ζ Per	1 Cas	κ Cas	62 Ori
1	$E_{(B-V)}$	0.09(0.02)	0.24(0.02)	0.27(0.02)	0.33(0.02)	0.30(0.02)	0.33(0.02)	0.21(0.02)	0.35(0.02)	0.44(0.02)
1	T_{01} (K)	81	63	-	61	48	57	82	104	-
2	$l^{(o)}$	157.4	158.9	160.8	160.4	160.4	162.3	110	120.8	189.7
2	$b^{(o)}$	-10.1	-16.7	-17.4	-13.1	-17.7	-16.7	-0.78	0.14	-0.86
3	D (pc)	165	284	238	544	452	301	621[1]	1009[1]	-
3	Err_D (pc)	145–191	227–377	192–316	394–877	328–730	246–389	-	-	
4	D_{ph} (pc)	168(42)	302(76)	254(64)	635(159)	529(133)	497(124)	-	-	-
5	D_{sp} (pc)	-	247(8)	311(9)	347(10)	166(5)	248(7)	-	-	-

Literature references:
1: Savage et al. 1977., except for HD23478: Krelowski et al. 1996 and HD41117: Krelowski & Sneden, 1993
2: SIMBAD database
3: Online Hipparcos catalogue.
4: Černis 1993.
5: Guetter 1977.

Table 2. Line profile fits for the λ6613 Å DIB, λ5895 Å Na I and the λ3934 Å Ca II lines. Velocities are heliocentric. Fit errors are given in parenthesis.

HD	24760	22951	23478	24912	23180	24398	218376	2905	41117
Name	ϵ Per	40 Per	-	ξ Per	o Per	ζ Per	1 Cas	κ Cas	62 Ori
fwhm (km s^{-1})	44.3(1.2)	50.8(2.2)	48.0(1.6)	49.9(0.4)	46.4(0.6)	42.4(0.8)	48.3(0.6)	51.5(0.8)	46.5(0.4)
V_C (km s^{-1})	1.4(0.8)	12.2(0.8)	11.6(1.0)	12.1(0.8)	12.2(0.6)	12.2(0.4)	-14.2(0.6)	-12.4(0.4)	12.7(0.4)
V_{DIBwm} (km s^{-1})	6(2)	16.5(3)	14.8(2)	16.3(8)	13.9(3)	15.4(3)	-13.8(2)	-13.1(2)	15.4(3)
V_{P1} (km s^{-1})	-10.7(0.8)	-7.6(0.8)	-11.2(0.8)	-8.2(0.5)	-5.4(0.8)	-5.7(0.2)	-32.4(0.5)	-23.5(0.7)	-4.5(0.5)
V_{P2} (km s^{-1})	7.8(0.6)	11.1(0.7)	10.6(0.8)	8.5(0.3)	12.1(0.4)	10.3(0.2)	-16.9(0.5)	-8.3(0.5)	10.9(0.5)
V_{P3} (km s^{-1})	15.8(0.7)	28.2(1.0)	28.3(0.5)	16.3(0.2)	27.7(0.2)	19.7(0.7)	-4.6(1.5)	2.9(1.3)	25.1(2.4)
V_{NaD_1} (km s^{-1})	6.7(0.2)	7.6(0.8)	9.4(0.8)	12.3(0.2)	13.6(0.8)	12.5(0.6)[a]	-	-	-
$V_{Ca\,IIwm}$ (km s^{-1})	12.7(0.6)[b]	13.3(0.6)	13.5(0.6)	12.1(0.6)[b]	12.2(0.6)[b]	12.5(0.6)[b]	-	-	-
V_{OH} (km s^{-1})	-	14.5(2.)[d]	14.9(1.0)[d]	-	14.8(1.0)[d]	13.1(1.0)[d]	-	-	-
$V_{H\,I}$ (km s^{-1})	-	12.3(1.)	14.9(1.0)[d]	10.4(1.0)[d]	13.8(1.0)[d]	12.2(1.0)[d]	-	-	-
V_{CO} (km s^{-1})	$-2.2(0.7)$[c]	-	15.4(0.7)[c]	15.8(0.7)[e]	15.3(0.7)[c]	14.2(0.7)[c]	-	-	-

Literature references:
[a] Welty et al., 1994
[b] Welty et al., 1996
[c] Ungerechts & Thaddeus, 1987
[d] Sancisi et al., 1974
[e] Smith et al., 1991

persion between the "centroid" DIB measurement (V_C) and the calculated DIB weighted mean velocity (V_{DIBwm}) is 1.7 km s^{-1} for the Per OB2 stars. Moreover, in both methods the velocity dispersion between Ca II and the DIB carrier is about 4.0 km s^{-1} (4.5 using V_C and 3.5 using V_{DIBwm}, respectively). The two methods are therefore equivalent to describe the DIB velocity distribution, within the error bars. When the DIB profile does not exhibit a strong asymmetric wing, the centroid, and weighted mean velocities are equal within the error bars. When asymmetries develop, the whole DIB profile is systematically shifted redward in wavelength (see Figs. 6 and 7) and the DIB carrier's velocity is reproduced less accurately with the weighted mean velocity, inducing a larger dispersion. As both methods are equivalent for the association stars, we chose the "centroid" velocity (less affected by possible DIB clouds overlap and/or temperature effects) to describe the DIB carrier spatial distribution throughout our study.

2.4. Fit limitations

As each fit was performed using the complete spectrum, the presence of remnants from stellar and/or telluric lines in the data increases the discrepancy between the data band profile and its parent population.

Another important limitation of the fitting functions for our purposes is linked to the line profiles themselves. The Na I and

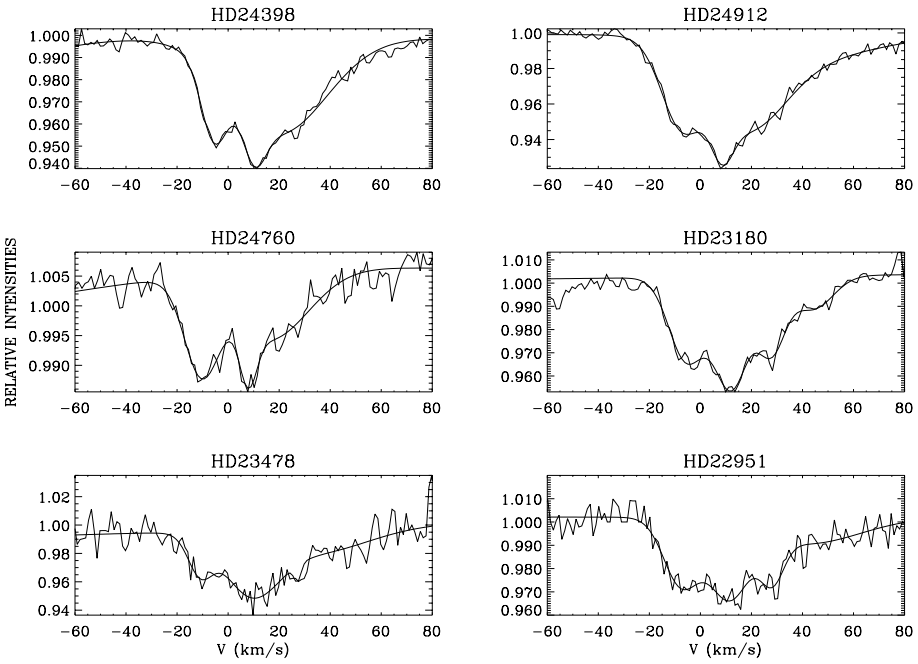

Fig. 1. The λ6613 Å DIB profiles toward the observed Perseus lines of sight together with their corresponding fits. The velocities are heliocentric and can be compared with the Ca II velocities (Fig. 6). This confirms that the triple peak substructures are intrinsic to the DIB (rotational contour of gas phase molecule) and not due to multiple cloud Doppler effects. Stars are named according to their HD numbers.

Ca II lines sometimes exhibit shoulders arising when multiple clouds overlap. The DIB profiles all show intrinsic asymmetries caused by the detected substructures, as well as a red wing. Our fitting procedure is based upon combinations of symmetric profiles (gaussians) which can reliably reproduce cloud overlapping effects and can resolve the molecular substructures. It, nevertheless, remains uncertain when wings appear in addition to multiple components as observed in all λ6613 Å DIB profiles of our program stars (see Fig. 1).

3. DIB distribution in the Perseus sample

3.1. Extinction in Perseus

3.1.1. Overall picture

Former studies of the interstellar extinction towards the Perseus OB2 association (Černis 1993) concluded that the total extinction in the visible (A_V) increases gradually from 0.4 to 2.7 mag showing two jumps. These 2 extinction steps correspond to 2 dominant extinction layers present in that region of the sky (see Figs. 2 and 3).

The first dominant layer is located at 160 (± 20) pc showing an *average* visual extinction A_V of 0.71 mag. It is generally attributed to an extension of the Taurus dark cloud (cloud (1)) in front of Perseus OB2.

The second dominant layer is located at 260 (± 20) pc and extends over 80 pc. It constitutes the so-called Perseus OB2 dark cloud complex. Its *average* visual extinction is 2.0 mag, after substraction of the extinction caused by the first layer. The OB2 association is a complex gathering of bright nebulae and dark clouds (see Fig. 3, (clouds (4), (5) and (6)). All studies agree on the existence of two dominant dense cores: IC 348 and NGC1333 embedding T Tauri stars. These two dense cores are located at a distance of 300 pc and have visual extinctions varying from 0.95 to 2.0 mag. A detailed study of the OH and H I emissions was performed to trace the dust distribution and correlate it with the gas and the distribution of the Per OB2 association stars (Sancisi et al. 1974, Sancisi 1974). Their results indicate the presence of two expanding shells: an H I shell with a 4° × 9° angular dimension (see Figs. 2 and 3, cloud (7)) and an OH shell having a 3° × 7° angular dimension (the OH shell was not reported for clarity). The OH shell is detected in the center of the H I shell, at l=160.5° and b=-17°. Sancisi et al. (1974) found an overall correlation between the OH emission and the extinction indicating that the OH distribution follows also the dust cloud distribution. The H I distribution does not correlate with extinction but does follow that of the OH clouds within 2 km s^{-1}. Sancisi et al. (1974) concluded that OH and H I and, hence, the dust and H_2 are spatially related in the Per OB2 association.

3.1.2. Association membership

We compared the distribution of our targets with respect to the cloud's distribution to better understand the Per OB2 line of sight properties, which are crucial to derive informations on the nature of the λ6613 Å DIB carrier. The program star names, distances, galactic coordinates, reddening estimations are reported in Table 1. The question of the Per OB2 association membership was recently revisited by De Zeeuw et al. (1999) applying the latest Hipparcos data to the study of nearby OB associations. The Per OB2 association's extension is $156 < l(°) < 164$ and $-22 < b(°) < -13$, which is quite off the galactic plane. Even-though our program stars are located in the Per OB2 angular region, their membership to the association is not straightforward and deserves a detailed investigation.

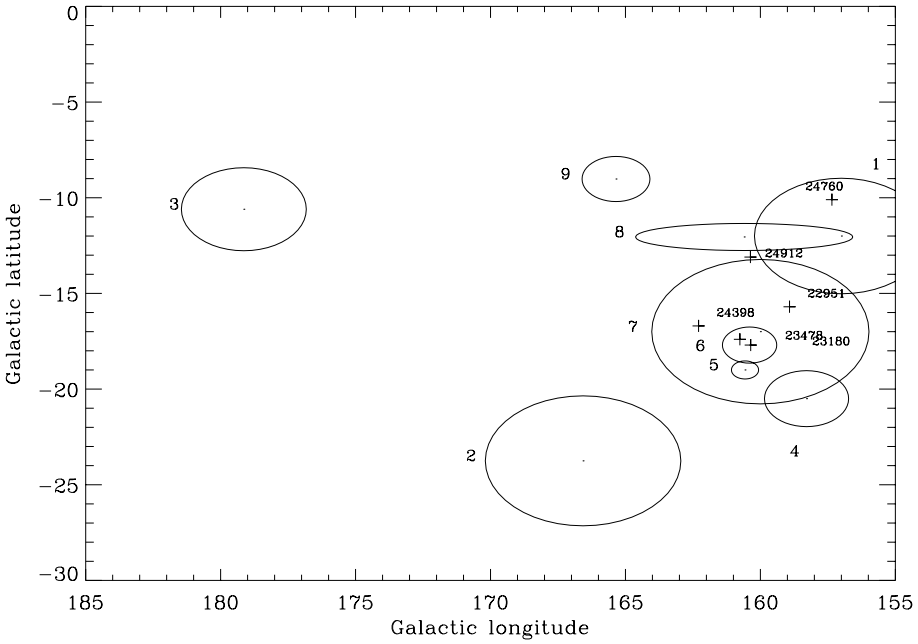

Fig. 2. Sketch of the cloud distribution in Perseus OB2 in galactic coordinates. The program star location is indicated with a (+). The cloud numbering is: (1) dark clouds around TMC-1, (2) Merope nebulae, (3) dark clouds around NGC1750/58, (4) NGC1333, (5) Barnard dark cloud B1, (6) IC348 dark cloud, (7) Per OB2 H I shell, (8) NGC1499, (9) NGC1579, (10) cloud stripe extenting from HD23180 to HD24912 seen on IRAS 60 μ maps, not reported for clarity.

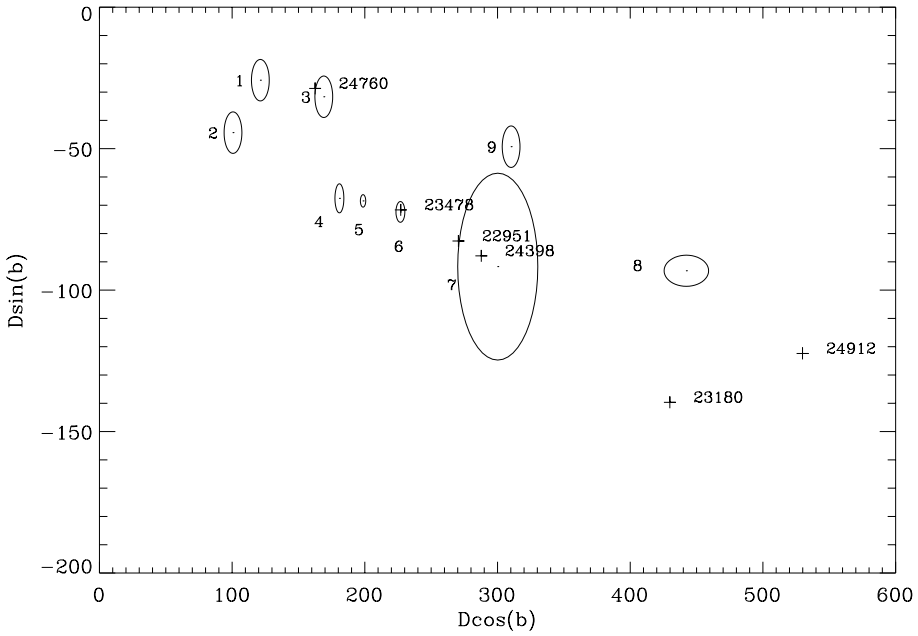

Fig. 3. Sketch of the clouds distribution in Perseus OB2 in a galactic cartesian diagram. The program star location is indicated with a (+). The cloud numbering is identical to Fig. 2.

1. HD24760 has a distance to the Sun and galactic coordinates which indicate, within the error bars, that this star is *not a member* of the association. It is seen in the **front** of the Perseus complex at a distance close to the distance of a Taurus arm remnant. IRAS 60 μm data also show that this region exhibits diffuse filamentary structures consistent with the low visual extinction of that line of sight (A_V=0.32 $\pm$ 0.2).
2. HD24912 is a runaway star, having a mean radial velocity of 67 km s^{-1} (against 19.4 km s^{-1} for the Per OB2 association stars, see De Zeeuw et al. 1999). The large distance indicates that the star is well beyond the dense cores in the direction of the association and is the exciting star of the California Nebulae NGC1499 (cloud (8) in Fig. 3). This star is therefore *a doubtful member* of the association.
3. HD22951, HD24398 and HD23478 have distances and mean radial velocities consistent with those of the association. Their visual extinctions are 0.84 ($\pm$ 0.2), 1.15 ($\pm$ 0.2) and 0.96 ($\pm$ 0.2), respectively ($R = A_V/E_{B-V}$=3.5($\pm$0.2), see Černis 1993). The galactic location further shows that they are situated close to the center of the association where the dense cores are detected. Their membership to the association is doubtless.
4. HD23180 has a mean radial velocity consistent with that of the association stars but a distance larger than the average association distance. This star is a *doubtful member* located

at the very back of the Perseus OB2 association, closely behind the overlapping dark clouds IC348, Barnard cloud B1 and the HD23180 to HD24912 cloud stripe (see Figs. 2 and 3, clouds (5), (6) and (10)).

3.2. Dust distribution

Previous studies were carried out to trace the dust components in the Galaxy associations using OH, CO and H I emission lines, which are dust and dense cores tracers. Detailed work on the dust distribution in the Per OB2 association was performed by Sancisi et al. (1974), Sancisi (1970 and 1974) and Ungerechts & Thaddeus (1987). Their studies led to the following summarized conclusions:

1. the H I component is detected in the form of an irregular shell with the same angular dimension as the association. Its positive velocity component shows a sudden increase with longitude where the dense cores are located (l=160.5°, b=−17°, V=15 km s^{-1}). It also shows a smooth velocity increase with latitude at the angular position of the star association. Its column density does not vary with extinction, indicating that the H I origin is not predominantly due to the dust located in the association. The presence of the runaway star HD24912 located in a dust-free line of sight points toward a supernovae remnant origin for the shell (Sancisi 1970).
2. OH is also detected in the form of a shell centered in the H I shell but having a smaller angular extent than the latter. It shows a good correlation with extinction and is therefore the *dust tracer* in the Per OB2 association. Like H I, OH shows a sudden velocity increase (V=16 km s^{-1}) at the same galactic coordinates than H I indicative of a peculiar motion of the dust which cannot be attributed to the differential galactic rotation of the Galaxy (Sancisi et al. 1974, Sancisi 1974).
3. the CO distribution (when available) matches that of OH within 1 km s^{-1} confirming the dust velocity distribution derived from OH measurements.
4. the dust and its tracing gas (OH) show an expansion motion with mean radial heliocentric velocity about 14 km s^{-1} in the direction of the association (against 11 km s^{-1} outside the angular spread of the Per OB2 stars). This indicates that the dust and corresponding gas components are kinematically linked to the star association. The dust experiences a velocity shift when observed toward the center of the association where the densest core (IC348) is located. As differential rotation of the Galaxy cannot account for this peculiar motion, one can infer that the dust acceleration is probably linked to the presence of T Tauri stars in that dense core. A careful study of that dense core and its dust component is, nevertheless necessary to verify that assumption.

In Fig. 4 and Fig. 5 we plotted the DIB centroid velocity distribution (V_C) derived from our measurements together with the velocities for OH, CO and H I from the literature, to investigate the link between the dust, its related gas and the DIB carrier. We overplotted the distribution of Ca II and Na I to trace the line of sight physical conditions in a: *(i)* velocity-distance diagram and *(ii)* velocity-galactic latitude diagram.

Each line of sight is labelled with the corresponding star HD number on the left handside. The interstellar atomic and molecular species were given symbols reported on the upper right corner of the diagrams. The measurement errors couldn't possibly be overplotted on the measurements themselves without making the diagrams unreadable. We, therefore, only reported the DIB ($\pm 1\sigma$) error measurement together with the Hipparcos distance error measurement on the right handside of Fig. 4. In Fig. 5 we also reported the DIB ($\pm 1\sigma$) error measurement. The galactic coordinate errors were not plotted because they are smaller than the symbols themselves. The ($\pm 1\sigma$) error measurements on the other intervening species are reported in parenthesis in Table 2. All velocities are heliocentric.

3.3. Gas distribution

Atomic and molecular lines are indicators of the ISM line of sight properties. As pointed out in the above section OH and CO are tracers of dust and dense core interiors. Atomic species such as Ca II or Na I trace diffuse gas as well as edges of clouds therefore probing different physical and chemical conditions. Fig. 6 and Fig. 7 show that Ca II is concentrated in two dominant overlapping layers with a mean radial velocity of 13.0 ($\pm$ 0.6) km s^{-1}.

The first layer is located in the front of HD24760 at around 140 pc, still part of the Taurus remnant arm. The second layer is located before the Per OB2 association at around 300 pc.

Fig. 6 pictures the Ca II cloud components taken from Welty et al. (1994) together with the data obtained in our survey (HD22951 and HD23478). Note that Welty's resolving power is R=600 000 (against R=110 000 in our survey). To assure consistency with the following analysis, we considered a default resolving power of R=110 000. Under that condition, one can see that:

- The Ca II clouds before HD24760 do overlap weakly those of the association.
- Towards HD22951, HD23478, HD23180 and HD24912, two main Ca II clouds dominate at 7 and 13 km s^{-1}.
- The 13 km s^{-1} velocity component is the only dominant component in HD24398.

The Ca II landscape ahead of the Per OB2 association seems, thus, formed of 2 main Ca II shells: the first has an extension of, at least, 5° × 5° and contains the 13 km s^{-1} velocity components; the second has a 3° × 4° minimum extension and contains the 7 km s^{-1} velocity component, considering our observational sensitivity.

The Na I cloud distribution cannot be studied as accurately as the Ca II distribution because of line saturation. One can nevertheless say that there are 2 Na I clouds. The first cloud lies in front of HD24760 linked to the Taurus arm. The second set of clouds is located in front of the Perseus association showing probable link to clouds (6) and (10). The Na I clouds are in gen-

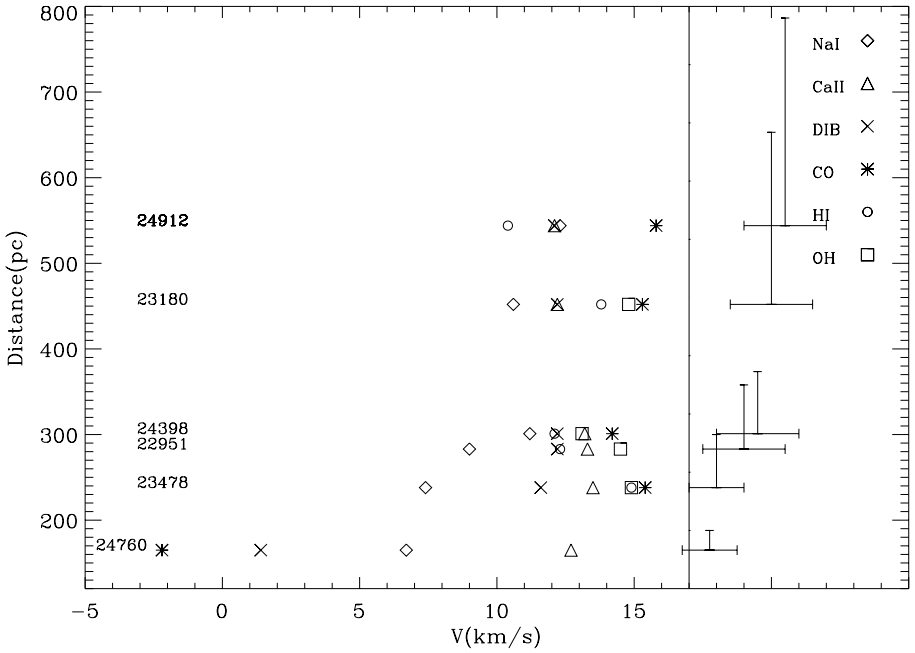

Fig. 4. The λ6613 Å DIB centroid distribution together with the Ca II, Na I, H I, OH and CO distributions vs star Hipparcos distance. The DIB and distance error measurements are reported on the right part of the diagram together with the interstellar species symbols. Velocities are heliocentric. The targets HD number are reported on the left side.

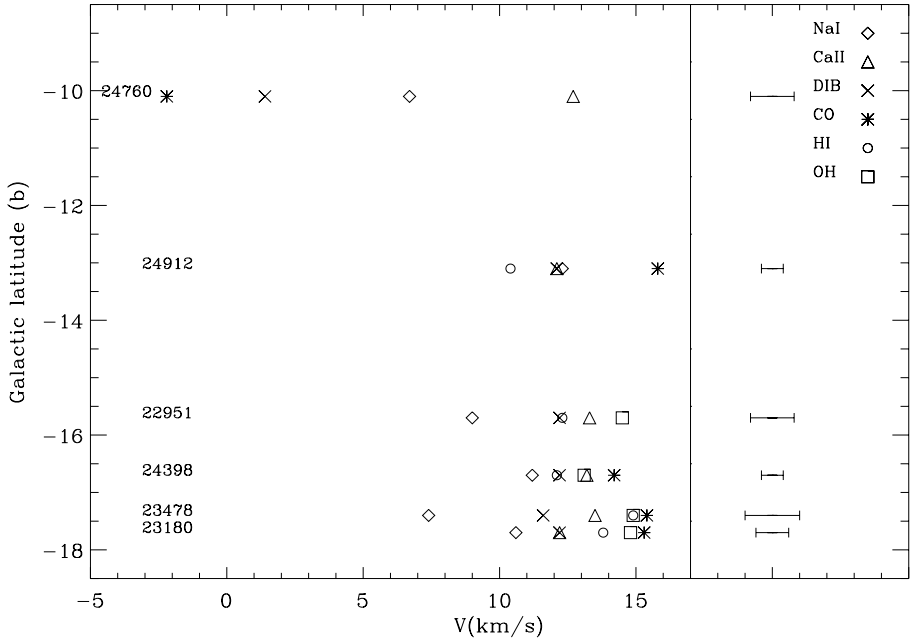

Fig. 5. The λ6613 Å DIB centroid distribution together with the Ca II, Na I, H I, OH and CO distributions vs star galactic latitude. The velocities are heliocentric. The DIB (1σ) error measurements are reported on the right part of the diagram together with the interstellar species symbols. The targets HD number are reported on the left side. HD22951 was displaced in +1 degree in galactic latitude for clarity.

eral moving slower than Ca II and are located before the Ca II clouds.

Moreover, the OH column densities for HD22951 and HD24398 represent only 15 to 30% of the HD23180 and HD23478 column densities, indicating an OH cloud extent (at mid maximum intensity) which is, hence, twice smaller compared to the Ca II and DIB clouds extent in column densities (see Table 3).

All studied atomic species show an overall expansion motion compatible with the motion of the dust-gas shells and clouds, stating their kinematical link to the star association.

3.4. The gas-cloud relation

A further analysis of Fig. 6, Fig. 3 and Fig. 2 allowed us to link spatially the Ca II main components (with R=110 000) to a few extinction clouds of the Per OB2 association.
(i) A cloud stripe (cloud (10)) extending from Barnard B1 (cloud (5)) to NGC1499 (cloud (8)) is crossed by all Per OB2 stars except for HD24398 which passes through the very edge of it. The 7 km s^{-1} Ca II component is present in equal intensity in all Per OB2 stars, except for HD24398 where it is almost below detection level. We infer that the 7 km s^{-1} Ca II component has an angular extent of at least $3^\circ \times 4^\circ$ and might be associated with this dust stripe (cloud (10)).

Table 3. Properties of the λ6613 Å DIB derived from our line profile fits. For each Perseus target we derived: the equivalent width W_λ (mÅ), the DIB, Ca II, H I and OH column densities (N) given in $(2.8\,10^{10}/\mathrm{f})\,\mathrm{cm}^{-2}$, 10^{10} atom cm^{-2}, 10^{20} atom cm^{-2} and 10^{14} mol cm^{-2} units, respectively. (f) stands for the DIB's oscillator strength. Errors are given in parenthesis.

HD	W_λ	N_{DIB}	$N_{\mathrm{Ca\,II}}$	$N_{\mathrm{H\,I}}$	N_{OH}
24760	62(15)	1.6(0.7)	39(4)	3(1)	-
22951	167(17)	4.3(0.4)	140(17)	12(1)	0.3(0.15)
23478	191(19)	4.9(0.5)	98(11)	9(1)	1.0(0.15)
24912	280(30)	7.2(0.6)	184(18)	20(1)	0.3(0.15)
23180	170(17)	4.40(0.4)	124(13)	10(1)	2.0(0.15)
24398	183(21)	4.7(0.5)	91(10)	12(1)	0.3(0.15)

Table 4. Estimation of the DIB to Ca II, H I and OH ratios, respectively. (f) stands for the DIB oscillator strength. Errors are given in parenthesis.

HD	DIB / Ca II $(2.8/f)$	DIB / H I $(2.8\,10^{-11}/f)$	DIB / OH $(2.8\,10^{-3}/f)$
24760	0.04(0.02)	5.3(2.0)	-
22951	0.03(0.01)	3.6(0.6)	1.5(0.9)
23478	0.05(0.01)	5.5(1.0)	0.5(0.1)
24912	0.04(0.01)	3.6(0.5)	2.4(1.0)
23180	0.04(0.01)	4.4(0.8)	0.22(0.04)
24398	0.05(0.01)	3.9(0.7)	1.6(0.8)

(ii) Similarly, cloud (6) (IC348) is crossed at proximity of its center by the 4 Per stars of our sample. It is therefore expected that the Ca II component observed towards those lines of sight has the same intensity and velocity in all of them. The 13 km s^{-1} Ca II component fullfils the above mentioned criteria at exactly the same velocity than the dust traced by OH. We can conclude that this component traces the Ca II layer linked to IC348 (cloud (6)).

We further show that the velocity component difference between HD23180 and HD23478 is consistent with the 21 km s^{-1} Ca II component appearing towards HD23180 in Fig. 6 and can therefore be attributed to the H I shell (cloud (7)), with similar H I and OH velocities.

Finally, this analysis led us to the conclusion that the distance stratification of the sampled stars and intervening clouds derived from the absorbing Ca II components confirms Fig. 2 and Fig. 3 schemes, despite the large uncertainties on the absolute distances (Hipparcos distances).

3.5. DIB carrier distribution

In order to better understand the DIB carrier behaviour we estimated its column density using our fit results.

Tables 3 and 4 summarize the fit-derived properties of the λ6613 Å DIB carrier in the studied Perseus region. In Table 3, we reported for each target: the DIB equivalent width (W_λ) in (mÅ), the DIB total column density (N) in $(10^{10})\,\mathrm{cm}^{-2}$ in (f) units, (f) being the DIB oscillator strength, the Ca II total column density (Welty et al. 1994), the H I column density and the OH column density. Table 4 reports the DIB to Ca II, DIB to H I and DIB to OH ratios, respectively, expressed in DIB (f) units. N was derived from the relationship:

$$N = \frac{1.13 * 10^{20} W_\lambda}{\lambda^2 f} cm^2, \quad (1)$$

where λ^2 and W_λ are given in (Å) and (f) is the oscillator strength of the molecule (White 1973). As the λ6613 Å DIB carrier has an unknown nature, we expressed the total column densities in (f) units to permit comparison of the DIB abundance from one line of sight to another and link it to the line of sight conditions. The DIB cloud distribution is represented via its centroid velocity (V_C, see Sect. 2.4). It follows the overall expansion motion observed in the Per OB2 association implying therefore that its history is linked to that of the other interstellar species and the star association. Fig. 4 and Fig. 5 show the existence of 2 distinct DIB clouds.

The first cloud is detected at 1.4 ($\pm$ 0.4) km s^{-1} toward HD24760. The low DIB density (i.e low interstellar material density) indicates its link to the first low extinction layer reported by Černis (1993) as the remnant of the Taurus arm (cloud (1)). HD24760 low extinction leads to a low self-shielded environment and the extreme proximity of the star leads to a very low absorbing material density accounting for a DIB column density 3 to 5 times lower than in the OB2 association targets (see Table 3).

The second DIB cloud is located *in average* at 12.0 ($\pm$ 0.4) km s^{-1} and extends over the entire Per OB2 association. Its steady column density (Table 3) further indicates that the carrier is possibly homogeneously distributed over the star association, indicative of DIB shell-like structures. Toward the association the *average* DIB shell velocity follows the *average* Ca II distribution within 2 km s^{-1} dispersion (rms), leading to the conclusion that the 2 species are spatially closely linked in the gas phase. Moreover, the DIB to Ca II total column densities ratio is constant (18% rms, within errors) toward the 6 sample stars (including the 2 non-members of the association HD24760 and HD24912, see Table 4). This indicates that the DIB column density varies proportionally with the Ca II column density. Furthermore, the DIB to H I ratio (see Table 4) is also invariant (19% rms, within errors) from one line of sight to the other. Those results lead to the important conclusion that among the interstellar species we considered in our study, Ca II and H I are good *tracers* of the λ6613 Å DIB carrier. On the contrary, the DIB to OH ratio is varying largely (70% rms, well above errors). This indicates the DIB carrier is more related to gas tracers (Ca II and H I) than dust tracers (OH). This result places a new constraint on that particular DIB carrier nature. As we have toward Per OB2 two dominant Ca II clouds (with R=110 000), we can further infer that we also have two overlapping DIB shells, one related to the Ca II in the cloud stripe (10) and one related to the Ca II in cloud (6). With an ionization potential of 11.9 eV, Ca II traces edges of dense clouds where UV pho-

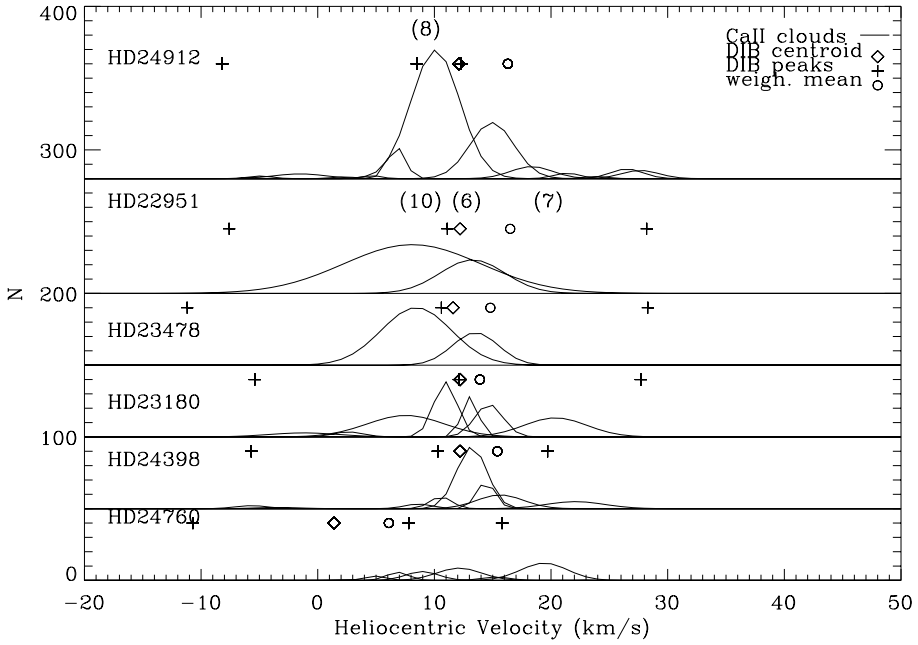

Fig. 6. The Ca II multiple cloud column density distribution (N) along the program star lines of sight. The diamond indicates the position of the DIB cloud using (V_C). The empty circle is the DIB weighted mean velocity V_{DIBwm}. We also reported the positions of clouds (6), (7), (8) and (10) showing the spatial link with some Ca II components.

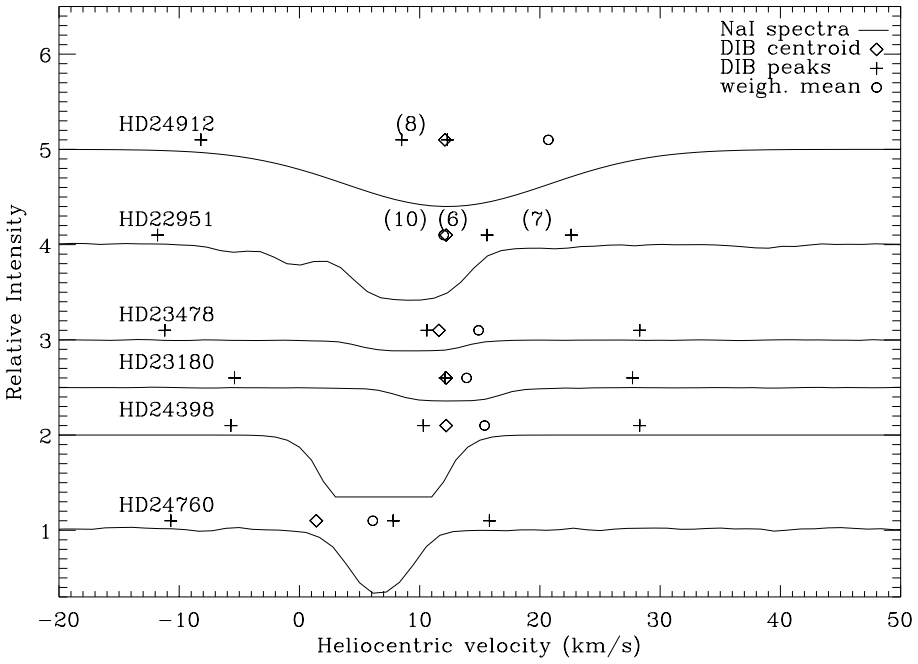

Fig. 7. High resolution Na I spectra (except for HD24912 R=25000) obtained during our campains. HD24398 was taken from Welty et al. (1994). Velocities are heliocentric.

tons do not suffer important shielding, this further supports the indication that the λ6613 Å DIB is due to a large carbonaceous ionized species (Sonnentrucker et al. 1997). Furthermore, the DIB average centroid velocity (12 km s^{-1}) also indicates that the DIB carrier follows the dominant Ca II component of IC348 (cloud (6)).

The case of HD24912 is puzzling. From Fig. 2, it seems that the HD24912 line of sight crosses the H I shell at its very edge, which is consistent with the "off" velocity position of the neutral hydrogen (10 km s^{-1}) in comparison with the H I distribution in the association (12 to 14 km s^{-1}). It is also reported as the exciting star of the reflection nebulae NGC1499 (cloud (8), therefore placed at proximity of HD24912 in Fig. 3). The DIB cloud velocity is consistent with that of the Per OB2 association which would lead to the conclusion that the shell extends over HD24912. Yet, the DIB column density toward HD24912 is 1.5 times higher than it is in the association shell. Knowing from former studies (see Herbig 1995) that there is a general DIB enhancement in this particular environment the alternative to the DIB cloud distribution toward HD24912 is the following: (i) either the DIB shells in front of the association extend over HD24912 and are part of NGC1499 forming an elongated DIB overall layer, (ii) or there is a third DIB cloud toward HD24912 having by chance, the same radial velocity as the association

DIB shells. Further study of that line of sight and an increase of the association star sample is needed to assess which explanation is the closest to reality.

3.6. Photochemistry in Per OB2

The extinction in the Per OB2 association ($A_v < 2.0$ mag) is characteristic of diffuse to translucent clouds. The chemistry network in that part of the ISM is based on ion-molecule reactions where C^+ is abundant and participates actively to the formation of large carbon molecules such as hydrocarbons. However, the build-up of those large molecules is quickly limited by photodissociation processes. Another indicated route to large carbon molecules invokes grain surface chemistry. PAHs and fullerenes are expected to exist mainly as "free" molecules. More complex aromatic molecules reside on dust grains and are formed by ultraviolet photo-processing in the diffuse ISM. The presence of soot material in carbon-rich stars, the spontaneous formation and the remarkable stability of the fullerene cage suggests the presence of fullerene compounds in interstellar space. PAHs are believed to be the most abundant free organic molecules, and to be remarkably stable. It is assumed that PAH molecules are partly produced in the outer atmospheres of carbon stars or desorbed from carbon-rich grains at the onset of the PPN-PN stage. Shock fragmentation of carbonaceous solid material can be an important source of aromatic molecules. During their evolution, gaseous PAHs react according to their environmental conditions. In denser regions and regions of high electron density, PAHs will remain neutral and hydrogenated. The strength of the local ultraviolet radiation field determines their degree of ionization, dehydrogenation, fragmentation and destruction. To complete the evolutionary cycle, PAH molecules may be accreted back in the solid phase on grains in dense clouds. Results from the Infrared Space Observatory (ISO) confirm the ubiquitous presence of aromatic structures in space. A strong link between gaseous PAHs as well as solid aromatic structures is suggested by recent ISO observations of HII regions and circumstellar environments (Verstraete et al. 1996).

In the case of the Per OB2 association, we found out that the DIB cloud velocity behaviour is not linked to that of the dust tracer (OH) as a function of longitude. This means: (i) either that the DIB carrier is *not* historically linked to the dust grains at all, (ii) or that the DIB carrier originating from grains has lost memory of the dust behaviour via interaction and/or degradation. The fairly large number of physical and chemical pathways occuring in the ISM does not allow to solve that issue, at the present time.

As already mentioned, Fig. 6 and Fig. 7 show the Ca II and Na I cloud distributions in the program star lines of sight. For each line of sight, we overplotted the DIB centroid velocity ($V_{\rm C}$, $\diamond$), the DIB weighted mean velocity ($V_{\rm DIBwm}$, o) and the substructure peaks ($V_{\rm P1\text{-}3}$, $+$).

The substructure peaks have a typical separation of 0.33 Å (between P_1 and P_2) and 0.22 Å (between P_2 and P_3) which are larger than the expected separation due to Doppler effects (0.13 Å) and, therefore, do not show any link to any of the Ca II or Na I cloud components. Furthermore, the relative strength of the 2 dominant Ca II components is such that the secondary dominant component does not exceed 30% of the total Ca II column density. Considering the relation existing between Ca II and the DIB carrier, the secondary DIB cloud column density should not exceed 30% of the total DIB column density for each line of sight. Hence, a Doppler effect would affect the DIB profile, but not in a dominant way. However, the detection of physical changes in these DIB substructures requires higher S/N data for deconvolving the effects of cloud Doppler velocities and is better done when comparing physically different single clouds (Ehrenfreund & Foing 1996)

Those new results reinforce the assumption that the DIB substructures arise predominantly from ro-vibrational transitions. Under that assumption, the peak substructures can be interpreted as P, Q and R rotational branches.

In this framework, a variation of the peak separation is expected with increasing temperature. In Fig. 6 and Fig. 7 a velocity shift between the centroid velocity and the Q branch seems to follow the temperature variation (see Table 1). However the asymmetries also reflect, to a lesser extent with our sensitivity, a Doppler effect induced by the two probable DIB shells we inferred, linked to the cloud stripe (10) and the cloud (6), respectively. Further discussion about the temperature effect on the λ6613 Å DIB profile is needed and will be pursued elsewhere.

4. Conclusion

We compared the λ6613 Å DIB velocity distribution to that of the interstellar Ca II, Na I, H I and to the dust distribution traced by the OH and CO gas components toward a 12.5° sky area of the Perseus OB2 association.

We used the molecular emission lines to trace the kinematics of the association and the atomic lines to derive information on the line of sight properties, crucial to better constrain the nature of the λ6613 Å DIB carrier.

Several new results are drawn from that study:

(i) The λ6613 Å DIB carrier follows the overall expansion motion of the atomic and molecular gas linked to the star association.
(ii) The λ6613 Å DIB carrier is detected in *two distinct* clouds. The first cloud has a velocity of 1.4 ($\pm$ 0.4) km s^{-1} and is part of the Taurus remnant arm ahead of HD24760.

The second DIB concentration is located in front of the Per OB2 association. It shows shell-like structures extended angularly over the whole association. The shells average velocity has a value of 12.0 ($\pm$ 0.4) km s^{-1} and an average DIB column density of 2.6 10^{10}($\pm$0.5) cm^{-2} in (f) units. This indicates the possible homogeneity of the DIB carriers distribution over the association.
(iii) Toward HD24912, the DIB velocity is similar to that of the association shell but its column density is 1.5 times larger. This means that, either we deal with a third different DIB layer having by chance the same velocity than the DIB association

shells, or the DIB shell extends over HD24912 and we actually trace a change in the physical conditions in that line of sight.
(iv) The dust mainly traced by OH and CO also shows the overall association expansion.
(v) Previous studies showed that the H I lines exhibit a sudden velocity increase toward the center of the association where the densest cores are located, indicative of the genetic link existing between the gas and the Per OB2 association stars.
(vi) The DIB distribution lies within 3.5 km s^{-1} of the dust/OH distribution, stating the good mixing of gas and dust toward the association. Nevertheless, the DIB to OH column density ratio is not independent of the line of sight, indicating that the λ6613 Å DIB carrier is not linked to the OH/dust component in a straightforward way as it is with Ca II and H I. The DIB distribution furthermore shows, an extent about twice as large as the dust with our sensitivity.
(vii) A detailed study of the Ca II components distribution revealed the existence of *2 main* Ca II *shells* located in the front of the Per OB2 association stars, showing different extensions. Another set of Ca II clouds is seen toward HD24760 and belongs to a remnant of the Taurus arm located 200 pc ahead of the Per OB2 association clouds.
(viii) The DIB carrier *average* velocity follows that of Ca II and H I, within our small error bars, leading to the conclusion that the three species are spatially linked in the gas phase.
(ix) The ratios of the DIB total column density to the Ca II and H I total column densities are independent of the line of sight conditions. This leads to the important conclusion that Ca II and H I *trace* the λ6613 Å DIB in the Per OB2 association. This new result reinforces the assumption that the λ6613 Å DIB is a gas phase molecule with an ionization potential between 10 and 13 eV.
(x) The close link between the λ6613 Å DIB and Ca II also leads to the conclusion that there are probably two DIB shells linked to the two dominant Ca II absorbing layers located ahead of IC348. The Ca II and DIB absorption analysis indicates that each dust cloud can be associated with a larger gas sphere with an inner part dominated by OH while the outer edge is dominated by ionized species such as Ca II and possibly the DIB carriers.
(xi) We confirm that the λ6613 Å DIB triple peak substructure is not due to multiple clouds Doppler effect, but is intrinsic to the DIB carrier rotational contour profile, pointing to a large gas phase molecule (such as C-rings, PAHs or fullerenes, as proposed by Ehrenfreund & Foing 1996), which may be single ionized (in agreement with the estimated ionization potential). Further studies of this region by increasing the number of DIBs and the line of sight sample will help to further constrain the properties of the unidentified molecular carriers. A dedicated investigation of the HD24912 line of sight should be initiated to better understand the physics of that region and its link with the DIB carrier nature. Detailed studies of other OB associations is compulsory to further investigate the DIB to Ca II and DIB to H I ratio invariances and search for further links between interstellar atomic species and DIB carriers.

Acknowledgements. P. Sonnentrucker acknowledges support from MESR (Ministère de l'Enseignement Supérieur et de la Recherche, France) with a doctoral fellowship (n^o96067). The authors thank T. Appourchaux for helpful comments. They are also grateful to their referee for very useful comments. We thank the staff of OHP for help during the observations. P.S. also thanks the Solar System Division at ESTEC/ESA for financial and computing facilities support.

References

Adamson A., Whittet D.C.B., Duley W.W., 1991, MNRAS 252, 234A
Cami J., Sonnentrucker P., Ehrenfreund P., Foing B.H., 1997, A&A 326, 822
Černis K., 1993, Baltic Astronomy Vol. 2, 214
De Zeeuw P.T., Hoogerwerf R., De Bruijne J.H.J, Brown A.G.A., Blaauw A., 1999, AJ 117, 354
Ehrenfreund P., Foing B.H. 1996, A&A 307, L25
Foing B.H., Ehrenfreund P., 1994, Nat 369, 296
Foing B.H., Ehrenfreund P., 1997, A&A 317, L59
Guetter H.H., 1977, AJ 82, 8
Herbig G.H., 1995, ARA&A 33
Jenniskens P., Ehrenfreund P., Foing B.H., 1994, A&A 281, 517
Kerr T.H., Hibbins R.E., Miles J.R., et al., 1996, MNRAS 283, L105
Kerr T.H., Hibbins R.E., Fossey S.J., Miles J.R., Sarre P.J., 1998, ApJ 495, L941
Krelowski J., Walker G.A.H., 1987, ApJ 312, 860
Krelowski J., Sneden C., 1993, PASP 105, 1141
Krelowski J., Megier A., Strobel A., 1996, A&A 308, 908
Krelowski J., Schmidt M., 1997, ApJ 477, 209
Ó Tuairisg S., 1998, European Master Thesis: A deep reference survey of Diffuse Interstellar Bands
Salama F., Bakes E.L.O., Allamandola L.J., Tielens A.G.G.M., 1996, ApJ 458, 621
Sancisi R., 1970, A&A 4, 387
Sancisi R., 1974, In: Kerr F.J., Simonson S.C. (eds.) Galactic radio astronomy. IAU Symp. 60, p. 115
Sancisi R., Goss W.M., Anderson C., Johansson L.E.B., Winnberg A., 1974, A&A 35, 445
Sarre P.J., Miles J.R., Kerr T.H., et al., 1995, MNRAS 277, L41
Savage B.D., Drake J.F., Budich W., Bohlin R.C., 1977, ApJ 216, 291
Smith A.M., Bruhweiler F.C., Lambert D.L., et al., 1991, ApJ 377, L61
Snow T.P. Jr., Cohen J.G., 1974, ApJ 194, 313
Sonnentrucker P., Cami J., Ehrenfreund P., Foing B.H., 1997, A&A 327, 1215
Sonnentrucker P., Foing B.H., Ehrenfreund P., 1998, Adv. Space Res., in press
Tulej M., Kirkwood D.A., Pachkov M., Maier J.P., 1998, ApJ 506, L69
Ungerechts, Thaddeus, 1987, ApJS 63, 645
Welty D.E., Hobbs L.M., Kulkarni V.P., 1994, ApJ 436, 152
Welty D.E., Morton D.C., Hobbs L.M., 1996, ApJS 106, 533
White R.E., 1973, ApJ 183, 81
Verstraete L., Puget J.L., Falgarone E., et al., 1996, ISO Special ISSUE, A&A 315, L337